A Computational Study on the Some Small Graphene-Like Nanostructures as the Anodes in Na−Ion Batteries

Mohammad Alipour, Fatemeh; Babazadeh, Mirzaagha*+

Department of Chemistry, Tabriz Branch, Islamic Azad University, Tabriz, I.R. IRAN

Vessally, Esmail*+

Department of Chemistry, Payame Noor University, Tehran, I.R. IRAN

Hosseinian, Akram

School of Engineering Science, College of Engineering, University of Tehran, P.O. Box 11365-4563, Tehran, Iran

Delir Kheirollahi Nezhad, Parvaneh

Department of Chemistry, Payame Noor University, Tehran, I.R. IRAN

ABSTRACT: *In this work, the interactions between the Na neutral atom and Na^+ ion and three nanostructures such as sumanene (SM), corannulene (CN), and nanosheet were investigated. The main goal of this work is to calculate the cell voltage (V) for Na−ion batteries, NIBs. The total energies, geometry optimizations, and density of states (DOS) diagrams were studied by using M06−2X level and 6−31+G(d,p) basis set. The DFT calculations indicated that the energy adsorption between Na^+ ion and nanostructures, E_{ad}, were increased in the order: SM-i > Sheet > CN-i > CN > SM. Nevertheless, the V_{cell} for SM has obtained the highest value. The V_{cell} of NABs are increased in the order: SM > CN > Sheet > SM-i > CN-i. This research theoretically described the possible uses of the mentioned nanostructures as anode the anodes in Na−ion Batteries.*

KEYWORDS: *Sumanene; Corannulene, Nanosheet, Anodes in Na−ion Batteries, DFT study.*

INTRODUCTION

Dry batteries play remarkable role in generation the electricity. The dry batteries, such as Zn−C, Ni−Cd, Ni−Zn and Na−ion batteries are very important because of readily uses. Some these batteries have drawbacks including environmental issues and transportable problems.

Lithium (Li) is a suitable anode metal for rechargeable batteries because of its low density, high specific capacity, and the lowest electrochemical potential [1]. However, the important issues involved for using Li-ion batteries, LIBs, are environmental issues the lifetime, cost, low-temperature performance of Li-ion batteries [2]. It can be suggested that Na-ion batteries (NIBs) may be a suitable replacement for LIBs because of the wide availability of sodium, its low cost and nontoxicity.

One of the important points for the development of sodium-ion batteries, NIB, is to find useful electrode materials with suitable electrochemical properties. Various nanostructures have been studied to use in the electronics, optics and sensor fields [3–5]. Some of the nanostructures

* To whom correspondence should be addressed.
+ E-mail: babazadeh@iaut.ac.ir ; vessally@yahoo.com
1021-9986/2021/3/691-703 13/$/6.03

are suitable to use in metal−ion batteries, MIB [6–9]. Recently, some efforts have been devoted to find some nanostructures such as nanosheet and nanotube [10], dichalcogenides [11], phosphorene [12], transition metal carbides or nitrides (MXenes) [13], nanocomposites [14] in ion-batteries.

Our goal in this work is to study the use of some carbon nanostructures including sumanene (SM), corannulane (CN) and nanosheet with different structures in NIBs as an anode. Different shapes and structures of nanostructures lead to different interactions between Na^+/Na and nanostructures which obtain various cell voltages. We investigated interactions between Na atom and Na^+ ion and three nanostructures including SM, CN and nanosheet (Fig. 1). Sumanene can be synthesized by oxidation of 1,5,9−trimethyltriphenylene [15]. Corannulane was first prepared in 1966 by organic multistep synthesis [16]. The synthesis and properties of corannulane have also reported in 1971 [17].

In continuing previous works [18], in this research, the cell voltage (V) of the three nanostructures such as SM, CN and nanosheet based on Na−ion battery was compared (Table 1). We expect that this reported computational results will aid the experimental chemists to improvement in Na−ion battery equipment.

COMPUTATIONAL METHODS

The total energies, geometry optimizations and density of states (DOS) for SM, CN and nanosheet were computed at the M06−2X level using 6−31+G(d,p) basis set [19]. All calculations were done in the G09 program [20]. During optimization process, all the atoms were optimized and the atoms were not fixed. All the structures are true minima on the potential energy surface and imaginary frequency was not obtained.

The chemical formulas of the nanostructures are SM, $C_{21}H_{12}$; CN, $C_{20}H_{10}$; and nanosheet, $C_{54}H_{18}$. Hydrogen atoms are used to cap the boundary carbon atoms of the nanostructures.

The Natural Bond Orbitals (NBO) of the Na^+/Na−nanocone complex were computed for the charge and hybridization study.

The Na and Na^+ adsorption energy is computed using the below equation:

$$E_{ad} = E_{complex} - E_{nanostructure} - E_{Na/Na+} + E_{BSSE} \quad (1)$$

where, $E_{nanostructure}$ is the energy of the nanostructures including SM, CN and nanosheet. The $E_{complex}$ is the energy of each nanostructure which Na or Na^+ adsorbed on the surface. The E_{BSSE} relates to the basis set superposition error which is calculated by the counterpoise method of *Boys* and *Bernardi* [21].

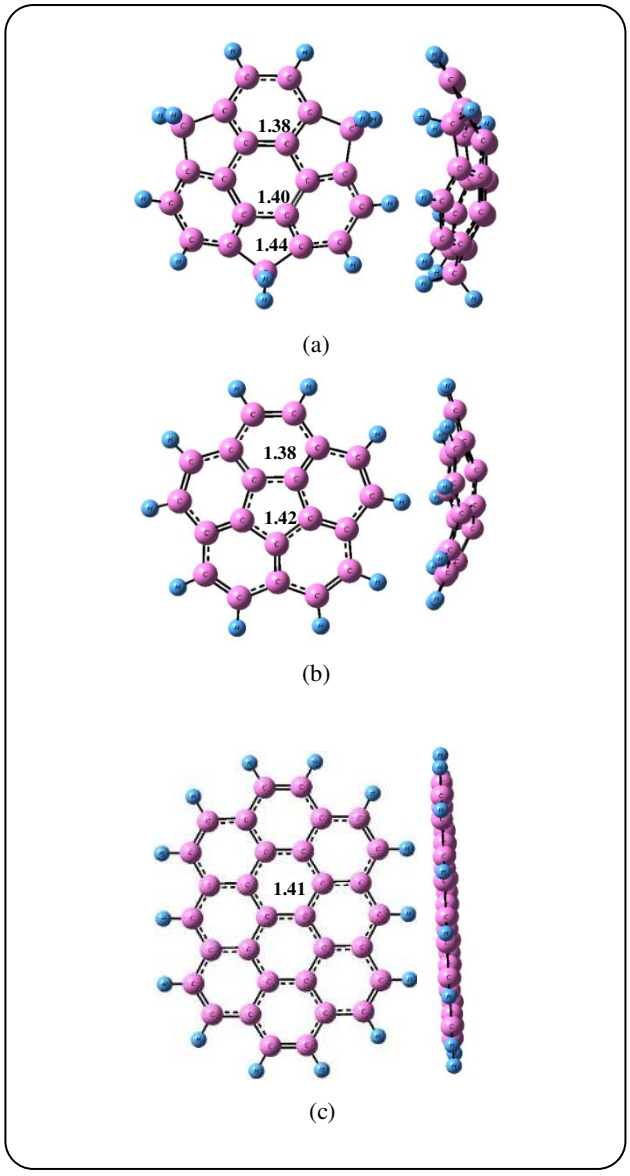

Fig. 1: Optimized molecular structures of (a) sumanene (SM); (b) corannulane (CN); (c) nanosheet.

The HOMO−LUMO energy gap (E_g) is calculated as:

$$E_g = E_{LUMO} - E_{HOMO} \quad (2)$$

where E_{LUMO} and E_{HOMO} are energies of HOMO and LUMO levels. The change of E_g is computed as follows:

$$\Delta E_g = [(E_{g2} - E_{g1})/E_{g1}] * 100 \quad (3)$$

Where, E_{g1} and E_{g2} are for nanostructures value and the complex value. This parameter indicates the electronic

sensitivity of the nanostructure to the Na/Na^+ adsorption. The Gaussum program has been used to compute the DOS plots [22].

RESULTS AND DISCUSSIONS

Following investigation of researchers in different fields of organic compounds [23-58] here, three kinds of nanostructures were designated to investigate their interactions with Na atom and Na^+ ion. Then, the cell voltage (V) of the three nanostructures based Na−ion battery (NIBs) was calculated and discussed. We check all regions at top of pentagon or hexagon ring for possible interaction with Na neutral atom and Na^+ ion. The global minima for all complexes were found in where the Na/Na^+ located in middle top of the pentagon or hexagon rings.

For SM and CN, the adsorption position of Na/Na^+ can be on concave and convex faces (Figs. 2, 5, 7 and 9). It would be important in compare the calculated data for both concave and convex faces. The interaction between Na^+ and SM in concave face is more (−2.08 kcal/mol) than convex surface. The interaction between Na^+ and CN in concave surface is slightly more (−0.47 kcal/mol) than convex surface.

Adsorption of Na/Na^+ over the sumanene

The core of SM is a benzene ring and the borderline consists of cyclopentadiene and benzene rings which is shown in Fig. 1 [59]. SM has a bowl−shaped with a bowl depth of 1.18 angstrom [59]. The six hub carbon atoms are pyramidalized by 9° and SM shows bond lengths (from 1.38 to 1.43 angstrom).

The HOMO and LUMO energies are −6.95 and −0.29 eV, respectively; thus the HOMO−LUMO gap energy is 6.67 eV (Table 1). In order to investigate the behavior of adsorption of Na^+/Na on SM, we must study all possibilities of the interaction between Na^+/Na and both inside or outside the bowl.

Adsorption of Na/Na+ outside the bowl of sumanene

The Na^+ ion and Na atom were optimized above the plane of the six−membered ring in SM with distances of 2.69 and 3.37 Å from carbon atoms, respectively (Fig. 2). This indicates a good interaction between SM and both Na^+ ion and Na neutral. The adsorption energy, E_{ad}, of the Na^+ ion on the SM is −32.34 kcal/mol that is larger than that of the Na neutral (−4.60 kcal/mol) (Table 1). Higher interaction between SM and Na^+ ion attributed to an interaction between Lewis base and Lewis acid.

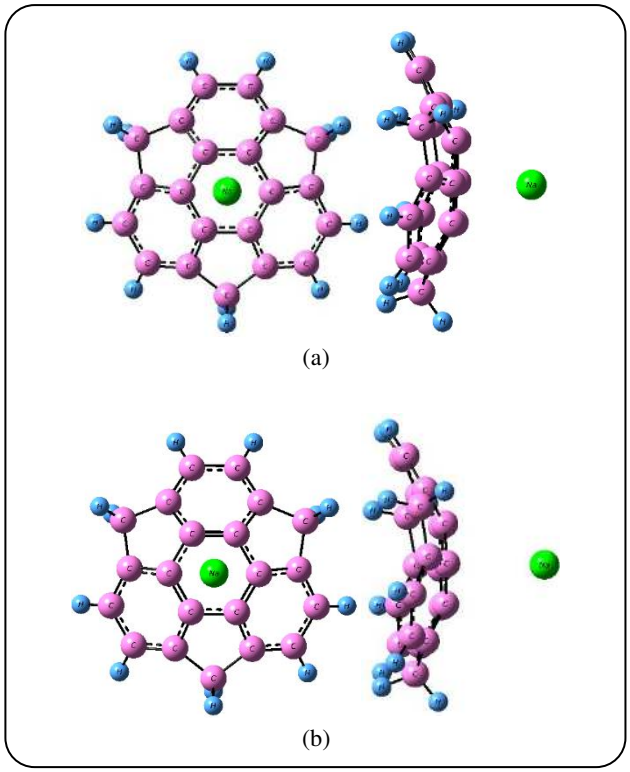

Fig. 2: Optimized structures of Na^+ and Na−SM complexes. (a) Na^+−SM complex (b) Na−SM complex. Pink, green and blue balls are carbon, sodium and hydrogen atoms.

The purpose of frontier molecular orbital analysis from the changes of the orbital level is to find which orbitals play main role in the interactions between nanostructures and Na atom or Na^+ ion.

The HOMO and LUMO change to the lower energies for the SM−Na^+ complex (Fig. 3). The HOMO and LUMO levels stabilized by Na^+ adsorption on SM in where the stabilization is sharp for LUMO level. The LUMO level mainly stabilized from −0.29 eV in SM to −4.62 eV in the SM−Na^+ complex (Table 1), cause to slightly diminish in the E_g (∼−10.5%) amount. The variations in HOMO, LUMO and E_g values are illustrated in Fig. 3 by density of state (DOS) diagrams. The partial density of states, PDOS, evidently shows that a new level created at the E_g gap of pristine which arises from Na^+ cation; decrease slightly in E_g of the Na^+−SM complex (Fig. 4).

The influence of atomic Na adsorption on the electronic aspects of SM−Na is unlike from that of SM−Na^+. Different to the Na^+ adsorption, the Na adsorption mainly leads the SOMO unstable because of being an unpaired electron in HOMO of the SM−Na complex. The amount of the SOMO level is changed

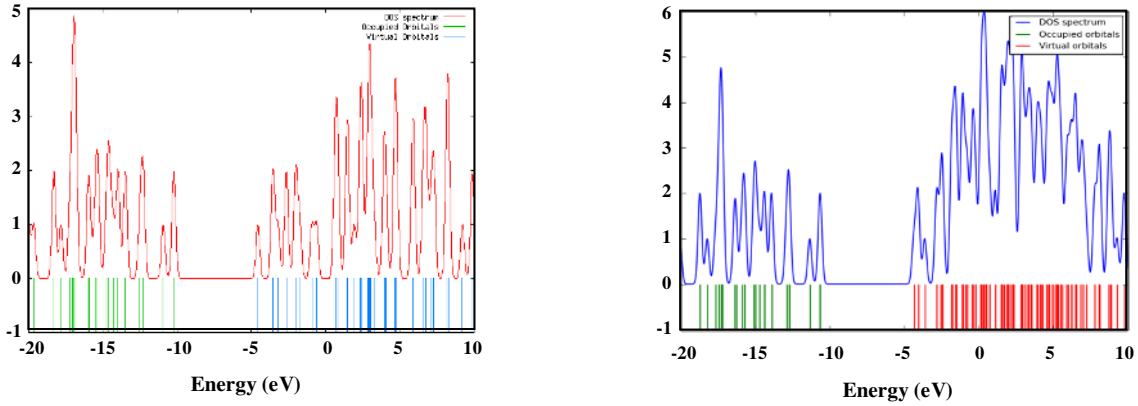

Fig. 3: Density of states (DOS) plot of SM (right) and Na^+− SM complex (left).

from −6.95 to −3.54 eV which is singly occupied. In consistent to the sharp energy change, the shape of HOMO is changed mainly by transferring to the adsorbing region. The energy amount of the LUMO level is slightly changed from −0.29 to −0.52 eV as shown in Table 1 and Fig. 4. The E_g (3.01 eV.) amount is significantly narrowed by about 53.0%, demonstrating that the effect of Na adsorption on the E_g is much more than that of the Na^+ adsorption. The partial density of states, PDOS, (Fig. 4) obviously shows that a new level formed at the E_g gap of pristine mostly arises from the Na neutral which causes to diminish mainly in E_g of Na−SM complex.

From the analysis of Partials Density of States (PDOS) plot of Na^+− SM and Na− SM, the electronic charge transfer could be explained that a new level produced from Na^+ cation at the LUMO area leads to decrease slightly in E_g of the Na^+−SM complex as well as increase the electronic charge transfer from HOMO of SM to LUMO of Na^+. In the Na−SM complex, Na atom interaction on SM produce an unstable SOMO which leads to increase the electronic charge transfer. The electronic charge transfer for the Na−SM complex is more than the Na^+−SM complex because the E_g for the Na−SM complex is less than the Na^+−SM complex.

The DFT calculations described that the *p* character of carbon atoms in the six−membered ring increases during adsorption of Na^+ since those carbon atoms intend to interact with the Na^+ cation. Strong interaction between π electrons of the six−membered ring and Na^+ cause to increase of the *p* character of carbon atoms and consequently to an increase of the bond length distance from 1.38 in pristine to 1.41 Å in Na^+−SM complex.

Adsorption of Na/Na+ inside the bowl of sumanene

The Na^+ ion and Na atom were optimized inside the plane of the six−membered ring of SM-i with lengths of 2.67 and 3.33 Å from carbon atom, respectively (Fig. 5). This indicates a good interaction between SM-i and both Na^+ ion and Na neutral. The adsorption energy, E_{ad}, of the Na^+ ion inside the SM-i is −34.42 kcal/mol that is larger than that of the Na neutral (−11.50 kcal/mol) (Table 1). These adsorption energies, E_{ad}, show a suitable interaction between SM and Na^+ ion as well as Na neutral inside the bowl of SM-i respect to outside the bowl of SM.

The changes in the HOMO and LUMO levels and E_g for Na/Na+ inside the bowl of SM-i is similar to outside the bowl of SM; stabilizing during Na^+ adsorption over SM which the stabilization is sharp for LUMO level. The LUMO level mainly stabilized from −0.29 eV in SM-i to −4.64 eV in the Na^+−SM-i complex (Table 1); decreasing in the E_g (∼−4.6%). The changes in HOMO, LUMO and E_g are illustrate in Fig. 6 by density of state (DOS) diagrams.

The Na adsorption mainly makes the SOMO unstable due to being an unpaired electron in HOMO of the Na−SM-i complex. This SOMO level decreased from −6.95 to −3.59 eV which is singly occupied. The energy of the LUMO level is slightly increased from −0.29 to −0.54 eV as shown in Table 1 and Fig. 6. As a result of large change in HOMO, the E_g is significantly narrowed by about 52.5%, indicating that the effect of Na adsorption on the E_g is much more than that of the Na^+ adsorption process.

Adsorption of Na/Na+ outside the bowl of corannulene

The corannulene nanostructure formed by a cyclopentane ring fused with four benzene rings named

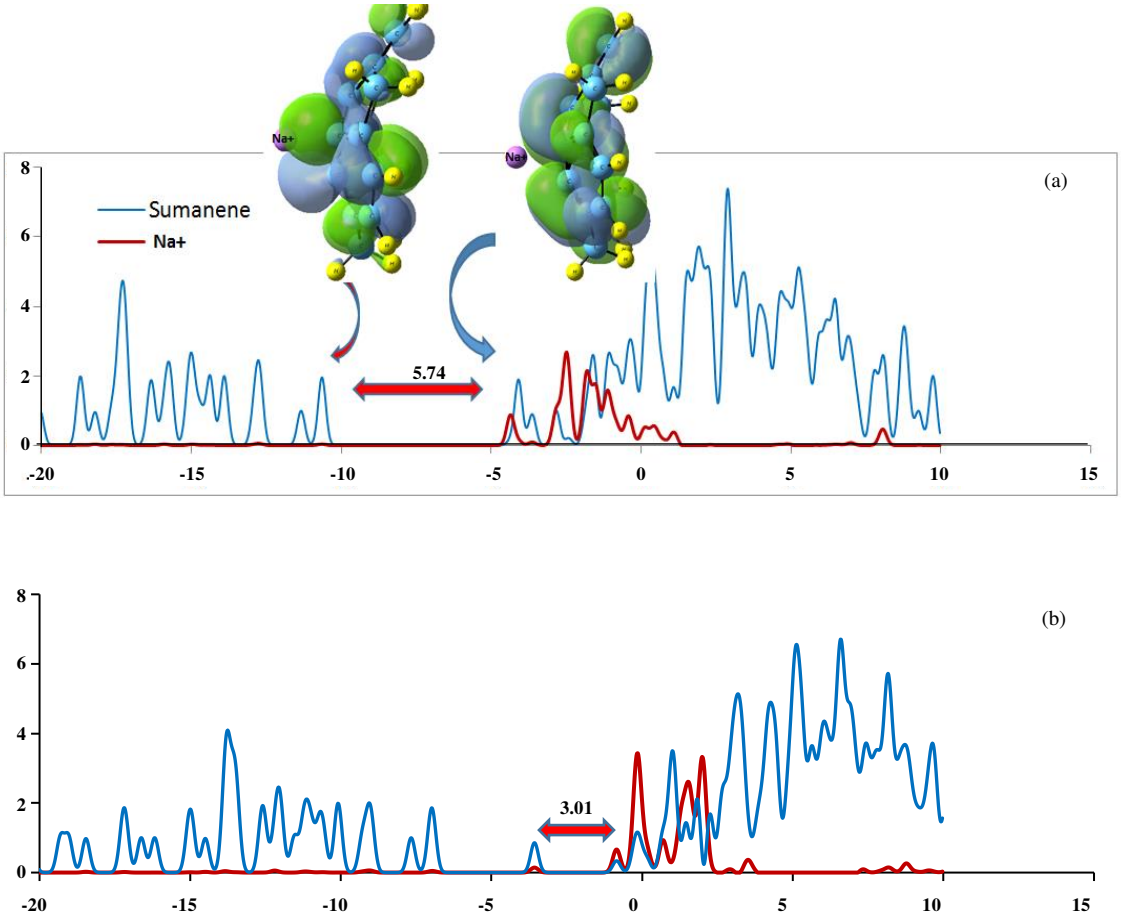

Fig. 4: Partials density of states (PDOS) plot of Na^+− SM and Na− SM. (a) PDOS plot of Na^+− SM (b) PDOS plot of Na− SM.

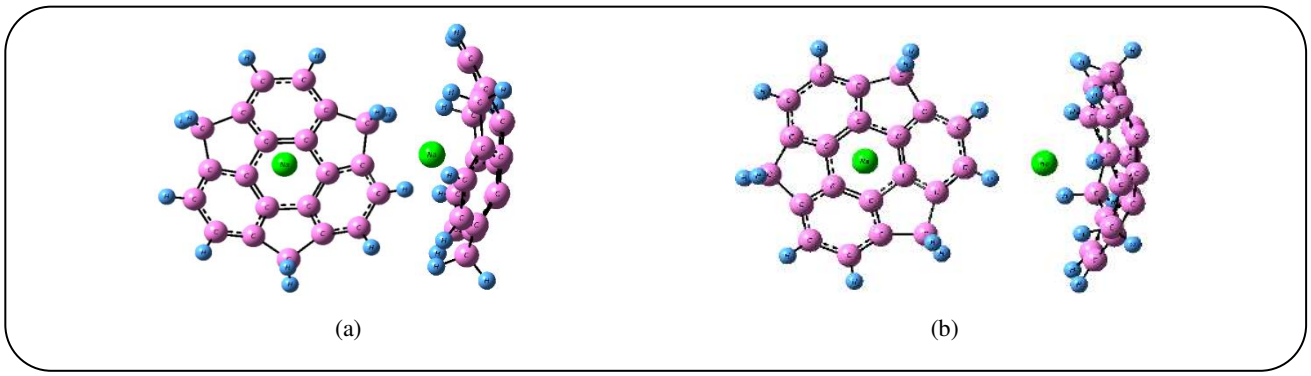

Fig. 5: Optimized structures of Na^+ and Na−SM-i complexes. (a) Na^+−SM-i complex (b) Na−SM-i complex. Pink, green and blue balls are carbon, sodium and hydrogen atoms.

as a buckybowl. The CN nanostructure have a bowl−to−bowl inversion with a barrier energy of 10.2 kcal/mol at −64 °C [60]. The Na^+ ion and Na atom were occurred above the plane of the five−membered ring of CN with distances of 2.66 and 2.56 Å from carbon atom, respectively (Fig. 7). The adsorption energy, E_{ad}, of the Na^+ ion on the CN is −32.67 kcal/mol that is higher than that of the Na neutral (−6.46 kcal/mol) (Table 1). The interactions between CN and both Na^+ ion and Na neutral are stronger than those of surname.

The HOMO and LUMO levels shift to the lower energies (more negative) for the CN−Na^+ complex (Fig. 8)

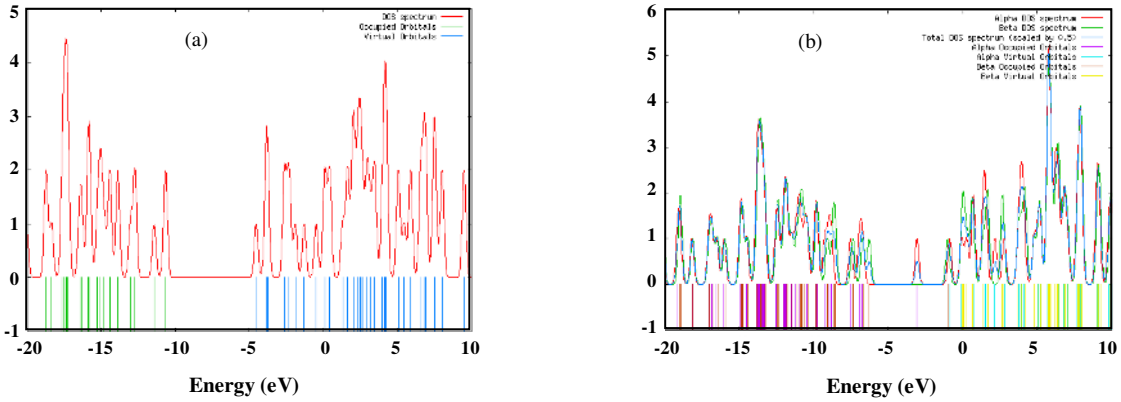

Fig. 6: Density of States (DOS) plot of (a) Na^+− SM-I; (b) Na−SM-i.

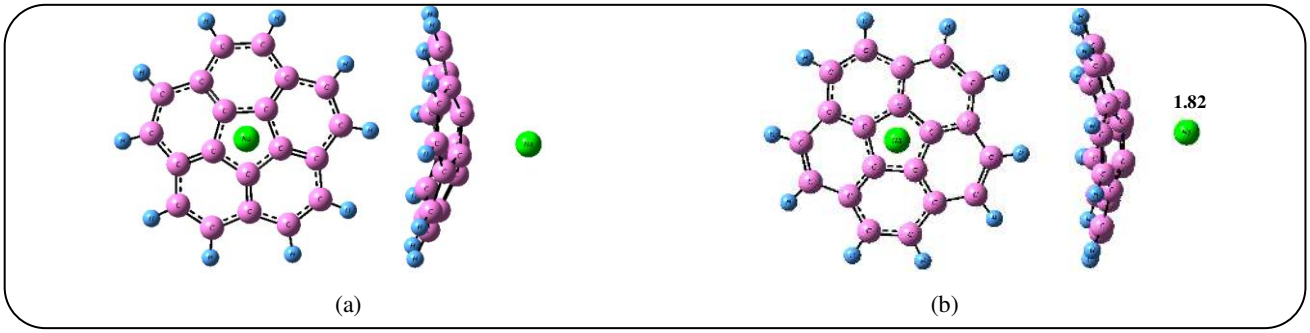

Fig. 7: Optimized structures of Na^+ and Na−CN complexes. (a) Na^+−CN complex (b) Na−CN complex, Distances are in Å. Pink, green and blue balls are carbon, sodium and hydrogen atoms.

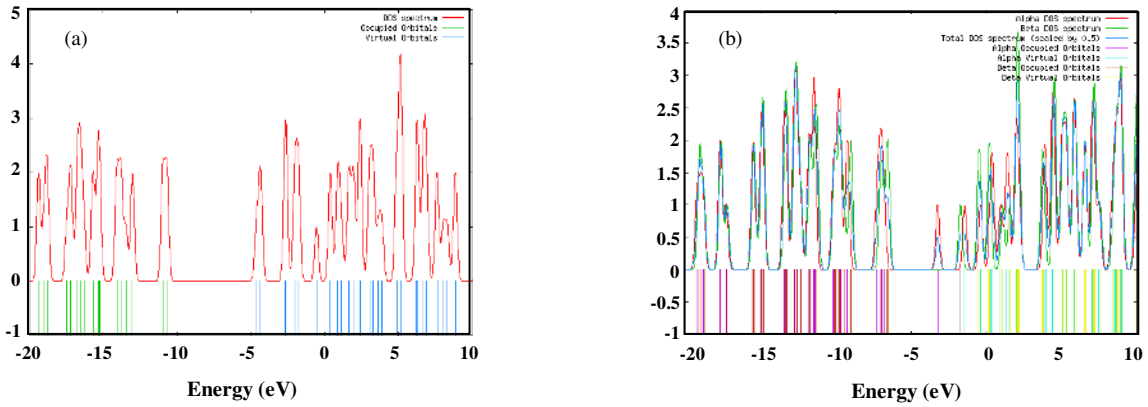

Fig. 8: Density of States (DOS) plot of (a) Na^+− CN; (b) Na−CN.

which shifting is sharp for LUMO level. The LUMO level considerably stabilized from −1.14 eV in CN to −4.66 eV in the CN−Na^+ complex (Table 1), leading to slightly diminish in the E_g (∼−7.3%). The changes in HOMO, LUMO and E_g are illustrated in Fig. 4 by density of state (DOS) diagrams. The density of states, DOS, obviously explains that a new peak formed at the E_g gap of pristine mostly arises from Na^+ cation which leads to diminish slightly in E_g of the Na^+−CN complex (Fig. 8).

The Na adsorption over CN mainly leads the SOMO unstable because of being an unpaired electron in HOMO of the CN−Na complex. This SOMO level is changed from −7.56 for CN to −3.51 eV for CN−Na complex which

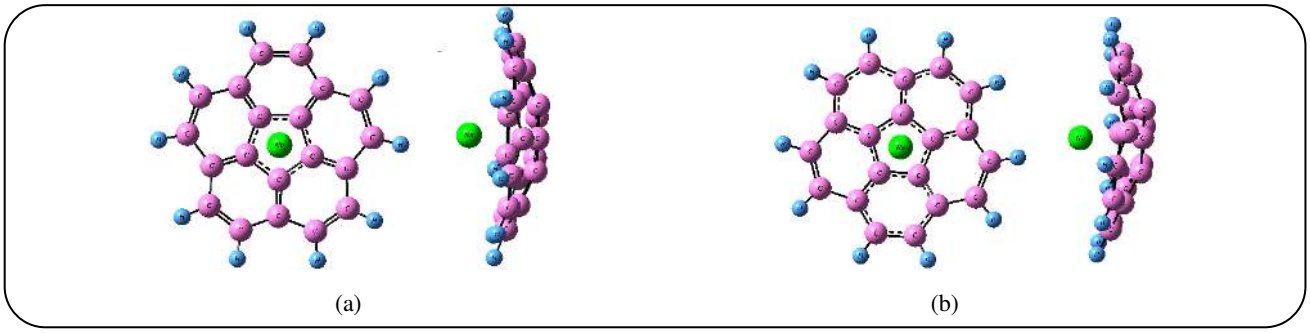

Fig. 9: Optimized structures of Na^+ and Na−CN−i complexes. (a) Na^+−CN-i complex (b) Na−CN-i complex. Pink, green and blue balls are carbon, sodium and hydrogen atoms.

is singly occupied. The shape of HOMO is changed remarkably by transferring to the adsorbing region. The energy of the LUMO level is unchanged as shown in Table 1 and Fig. 8. The E_g is significantly decreased by 71.2%, indicating that the Na adsorption changes the E_g much more than that of the Na^+ adsorption. The changes in HOMO, LUMO and E_g are demonstrated in Fig. 8 using Density of State (DOS) diagrams.

Adsorption of Na/Na+ inside the bowl of corannulene

The Na^+ ion and Na atom were optimized inside the plane of the five−membered ring of CN with distances of 2.66 and 2.56 Å, respectively (Fig. 9). The adsorption energy, E_{ad}, of the Na^+ ion inside the CN is −33.14 kcal/mol that is higher than that of the Na neutral (−12.85 kcal/mol) (Table 1).

The changes in the HOMO and LUMO levels and E_g for Na/Na+ inside the bowl of CN is more or less similar to outside the bowl of CN. The LUMO level considerably stabilized from −1.14 eV in CN to −4.85 eV in the Na^+−CN−i complex (Table 1); causing to slightly diminish in the E_g (∼−3.0%). The changes in HOMO, LUMO and E_g are illustrate in Fig. 10 by density of state (DOS) diagrams.

This SOMO level is changed from −7.56 for CN to −2.29 eV for Na−CN−i complex which is singly occupied. The energy of the LUMO level is almost slightly changed from −1.14 to −1.44 eV as shown in Table 1 and Fig. 10. As a result of large change in HOMO, the E_g is mainly narrowed by about −65.6%, indicating that the effect of Na adsorption on the E_g is much more than that of the Na^+ adsorption process.

Adsorption of Na/Na+ over nanosheet

The Na^+ ion and Na atom were optimized above the plane of the six−membered ring of nanosheet with distances of 2.68 and 2.62 Å, respectively (Fig. 11). The adsorption energy, E_{ad}, of the Na^+ ion on the nanosheet is −34.3 kcal/mol that is larger than that of the Na neutral (−10.81 kcal/mol) (Table 1).

The HOMO and LUMO levels for nanosheet changes to the lower energies for the nanosheet−Na^+ complex (Fig. 12). The LUMO level mainly stabilized from −1.59 eV in nanosheet to −4.63 eV in the nanosheet−Na^+ complex (Table 1), causing to slightly diminish in the E_g (∼−3.9%). The changes in HOMO, LUMO and E_g are illustrate in Fig. 12 by Density of State (DOS).

The Na adsorption mainly causes the SOMO unstable because of being an unpaired electron in HOMO of the nanosheet−Na complex. This amount of the SOMO level is changed from −5.95 to −3.67 eV which is singly occupied. The energy of the LUMO level is slightly changed as shown in Table 1. The E_g is significantly decreased by 58.4%, representing that the Na adsorption changes the E_g more than that of the Na^+ adsorption. The changes in HOMO, LUMO and E_g are demonstrated in Fig. 12 using density of state (DOS).

It was very interesting that distance of Na from CN plane is smaller than that of Na^+ while distance of Na from SM plane is larger than that of Na^+. It is seemed that the six-membered ring in SM is aromatic which there is a strong π-cation interaction that leads to decrease distance of Na^+ and SM plane while five-membered ring in CN is not aromatic and the carbon atoms of five-membered ring have slightly positive charge which leads to larger distance between Na+ and CN plane.

Comparison the nanostructures in the Na^+−ion batteries (NABs)

Three kinds of nanostructures proposed as an anode for the NIBs. The typical reactions in the anode and cathode are the following process [61]:

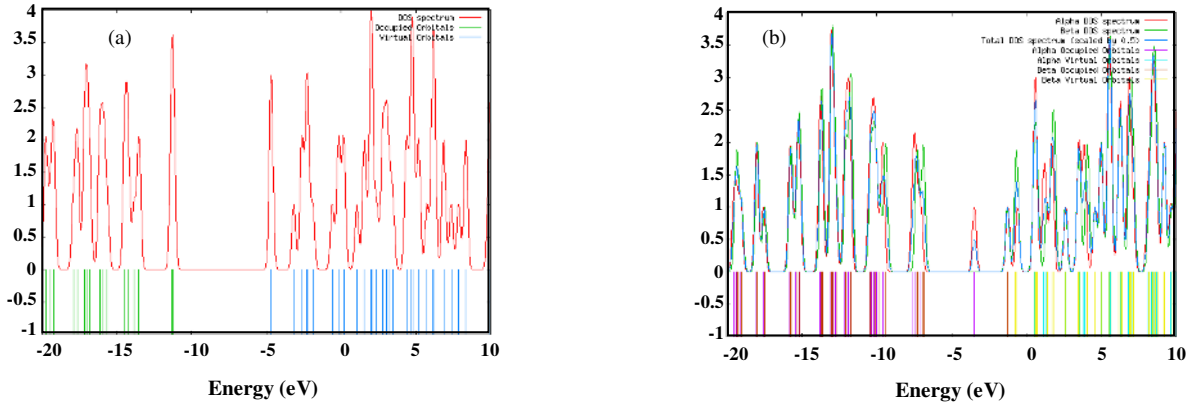

Fig. 10: Density of states (DOS) plot of (a) Na^+− CN-i; (b) Na−CN-i.

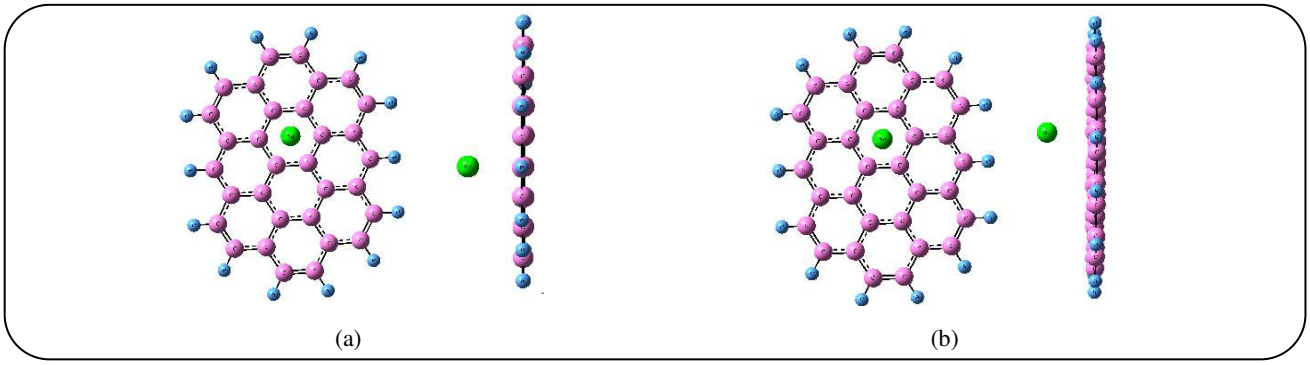

Fig. 11: Optimized structures of Na^+ and Na−Sheet complexes. (a) Na^+−Sheet complex (b) Na−Sheet complex, Distances are in Å. Pink, green and blue balls are carbon, sodium and hydrogen atoms.

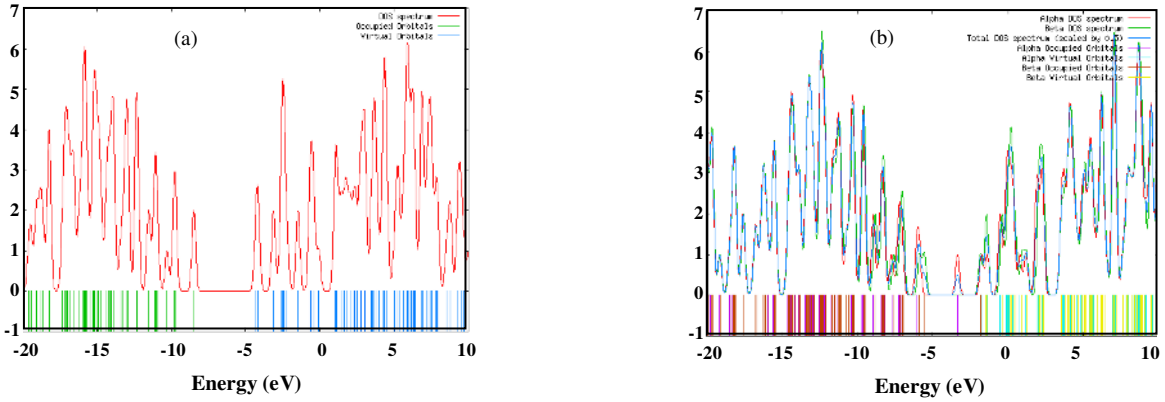

Fig. 12: Density of states (DOS) plot of (a) Na^+− Sheet; (b) Na−Sheet.

Anode: Na−nanostructure ↔ Na^+− nanostructure + e^- (4)

This reaction can be divided into several reactions that are presented below:

Cathode: $Na^+ + e^- \leftrightarrow Na$ (5)

The total reaction of the cell can be defined as:

$Na^+ + Na$−nanostructure ↔ Na^+−nanostructure + $Na + \Delta G_{cell}$ (6)

The Nernst equation is used to obtain the cell voltage (V_{cell}) as follows:

Table 1: The adsorption energies of atomic Na and Na^+ (E_{ad}, $kcalmol^{-1}$) on different nanostructures.

Nanostructure	E_{ad}	E_{HOMO}	E_{LUMO}	E_g	$\%\Delta E_g$	ΔE_{cell}	V_{cell}
SM	−−−	−6.95	−0.29	6.67	−−−	−−−	−−−
SM/Na	-4.60	-3.54	-0.52	3.01	-53.02	−−−	−−−
SM/Na^+	-32.34	-10.36	-4.62	5.74	-10.53	-27.74	-1.20
SM−i/Na	-11.50	-3.59	-0.54	3.05	-52.54	−−−	
SM−i/Na^+	-34.42	-10.76	-4.64	6.12	-4.59	−22.92	-0.99
CN	−−−	−7.56	−1.14	6.42	−−−−	−−−	−−−
CN/Na	-6.46	-3.51	-1.59	1.92	-71.16	−−−	−−−
CN /Na^+	-32.67	-10.84	-4.66	6.18	-7.35	−26.20	-1.14
CN −i/Na	-12.85	-3.74	-1.44	2.29	-65.58	−−−	
CN −i/Na^+	-33.14	-11.31	-4.85	6.46	-3.02	−20.29	-0.88
Sheet	−−−	-5.95	-1.59	4.36	−−−	−−−	−−−
Sheet/Na	-10.81	-3.67	-1.86	1.81	−58.41	−−−	−−−
Sheet/Na^+	-34.32	-9.16	-4.63	4.53	3.91	-23.51	−1.02

Energies of HOMO, LUMO, and HOMO−LUMO gap (E_g) in eV. ΔE_g indicates the change of E_g of nanostructures after the Na/Na^+ adsorption. The total energy change (ΔE_{cell}, kcal/ mol) and cell voltage (V) of the nanostructures based Na−ion battery.

$$V_{cell} = -\Delta G_{cell}/zF \quad (7)$$

Where, F and z are the Faraday constant (96500 C/mol) and charge of Na^+ (z=1, the cation in electrolyte), respectively. The ΔG_{cell} is the Gibbs free energy difference of the total reaction of cell. For DFT calculations at 0 K, it can be presented:

$$\Delta G_{cell} = \Delta E_{cell} + P\Delta V - T\Delta S \quad (8)$$

Theoretical storage capacity was achieved by comparing two relative interaction energies. One interaction energy is related to interaction between the Na^+ ion and nanostructure which strong interaction energy leads to high cell voltage. Another interaction energy is related to interaction between the Na atom and nanostructure which weak interaction energy leads to high cell voltage.

In previous reports we assume that the amount of volume and entropy contribution are very small (< 0.01 V) to the V_{cell} [62]. Therefore, the V_{cell} for Na^+– or Na–nanostructure can be determined by calculating the internal energy change (ΔE) from Eqs. (6) and (8) as follows:

$$\Delta E_{cell} \sim \Delta G_{cell} = E_{Na} + E_{Na+-nanostructure} - E_{Na+} - E_{Na-nanostructure} \quad (9)$$

Eq. (9) indicates that the strong interaction between Na^+ and nanostructure and weak interaction between Na atom and nanostructure obtain more negative and high ΔE_{cell}. In conclusion, the strong adsorption of Na^+ and weak adsorption of Na on the nanostructure lead to high V_{cell} (Table 1). The adsorption energy between Na^+ and nanostructures, E_{ad}, is increased in the order: SM-i > Sheet > CN-i > CN > SM. The ΔE_{cell}, and V_{cell} are calculated for three nanostructures which presented in Table 1 and schemed in Fig. 13. The ΔE_{cell}, and V_{cell} values for three nanostructures in NIBs changed in the same order: SM > CN > Sheet > SM-i > CN-i. The largest ΔE_{cell} and V_{cell} values of −27.74 kcal/mol and 1.20 V, respectively, belonged to SM. The V_{cell} for SM is the highest because the interaction between SM and the Na neutral is the lowest. The strong interaction between Na^+ and nanostructure and the weak interaction between the Na atom and nanostructure lead to higher V_{cell} amount of the NIBs−nanostructure. The ΔE_{cell} and V_{cell} for NIBs−nanosheet are −22.92 kcal/mol and 0.99 V, respectively, which are lower than the values of SM. The lowest V_{cell} value belongs to the NIBs−CN−i due to highest interaction between the Na neutral and CN−i. In general, the V_{cell} value for NIBs−nanostructures are from −0.88 to −1.20 V, makes these nanostructures

the promising candidates which could use to manufacture of the NIBs as anode. We can report that the interaction between the Na neutral and nanostructures play a significant role in V_{cell} respect to the interaction between the Na^+ neutral and nanostructures.

CONCLUSIONS

In this research, the adsorption of Na^+ and Na on three kinds of the nanostructures including sumanene (SM), corannulene (CN) and nanosheet was investigated to find a suitable anode of NIBs. The interaction between Na^+ and the surface of nanostructures is obviously stronger than that of the Na which reveals that these nanostructures are suitable for an anode of NIBs. The energy adsorption, E_{ad}, between Na^+ and nanosheet was the highest adsorption energy which E_{ad} were changed in the order: SM-i > Sheet > CN-i > CN > SM. However, the cell voltage, V_{cell}, was the highest for Sumanene. The changes in V_{cell} of NABs are in the order: SM > CN > Sheet > SM-i > CN-i. The interaction between Na^+ and Na and nanostructures play a remarkable role in determination of the cell voltage. The strong interaction between Na^+ and nanostructures and weak interaction between Na and nanostructures led to obtain a high V_{cell}.

Received : March 3, 2020 ; Accepted : Aug. 3, 2020

REFERENCES

[1] Xu W., Wang J., Ding F., Chen X., Lisybulin E., Zhang Y., Zhang J.−G., Scale-Up Production of High-Tap-Density Carbon/Mnox/Carbon Nanotube Microcomposites for Li-Ion Batteries with Ultrahigh Volumetric Capacity, *Energy Environ.. Sci.*, **7**: 513–537 (2014).

[2] Er D., Li J., Liguib M., Gogotsi Y., Shenoy V.B., Ti_3C_2 MXene as a High Capacity Electrode Material for Metal (Li, Na, K, Ca) Ion Batteries, *ACS Appl. Mater. Interfaces.,* **6**: 11173–11179 (2014).

[3] Siadati S.A., Vessally E., Hosseinian A., Edjlali L., Possibility of Sensing, Adsorbing, and Destructing the Tabun-2D-Skeletal (Tabun Nerve Agent) by C20 Fullerene and Its Boron and Nitrogen Doped Derivatives, *Synthetic Met.*, **220**: 606–611 (2016).

[4] Siadati S.A., Vessally E., Hosseinian A., Edjlali L., Determining the Status of Activity of Daily Living (ADL) and Instrumental Activity of Daily Living (IADL) in Healthy and Cognitive Impaired Elderlies, *Talanta.,* **162**: 505–510 (2017).

[5] Vessally E., Soleimani–Amiri S., Hosseinian A., Edjlal L., Bekhradnia A., Selective Detection of Cyanogen Halides by BN Nanocluster: A DFT Study, *Physica E.*, **87**: 308–311 (2017).

[6] Hosseinian A., Saedi Khosroshahi E., Nejati K., Edjlali E., Vessally E., A DFT Study on Graphene, SiC, BN, and AlN Nanosheets as Anodes in Na-Ion Batteries, *J. Mol. Model.*, **23**: 354- (2017).

[7] Nejati K., Hosseinian A., Edjlali L., Vessally E., The Effect of Structural Curvature on the Cell Voltage of BN Nanotube Based Na-Ion Batteries, *J. Mol. Liq.*, **229**: 167–171(2017).

[8] Subalakshmi P., Sivashanmugam A., CuO Nano Hexagons, an Efficient Energy Storage Material for Li-Ion Battery Application, *J. Alloys Compd.*, **690**: 523–531 (2017).

[9] Nejati K., Hosseinian A., Bekhradnia A., Vessally E., Edjlal L., Na-ion Batteries Based on the Inorganic BN Nanocluster Anodes: DFT Studies, *J. Mol. Graph. Model.*, **74**: 1–7 (2017).

[10] Jing Y., Zhou Z., Cabrera C.R., Chen Z.F., Graphene, Inorganic Graphene Analogs and Their Composites for Lithium Ion Batteries, Graphene, Inorganic Graphene Analogs and Their Composites for Lithium Ion Batteries, *J. Mater. Chem. A.*, **2**: 12104−12122 (2014).

[11] Hao J.Y., Zheng J.F., Ling F.L., Chen Y.K., Jing H. R., Zhou T.W., Fang L., Zhou M., Strain-Engineered Two-Dimensional MoS_2 as Anode Material for Performance Enhancement of Li/Na-Ion Batteries, *Sci. Rep.*, **8**: 2079 (2018).

[12] Li W., Yang Y.M., Gang Z., Zhang Y.W., Ultrafast and Directional Diffusion of Lithium in Phosphorene for High-Performance Lithium-Ion Battery, *Nano Lett.*, **15**: 1691−1697 (2015).

[13] Wang D.S., Gao Y., Liu Y.H., Jin D., Gogotsi Y., Meng X., Du F., Chen G., Wei Y.J., First-Principles Calculations of Ti_2N and Ti_2NT_2 (T = O, F, OH) Monolayers as Potential Anode Materials for Lithium-Ion Batteries and Beyond, *J. Phys. Chem.* C., **121**: 13025−13034 (2017).

[14] Kim S.K., Chang H., Kim C.M., Yoo H., Kim H., Jang H.D., Fabrication of Ternary Silicon-Carbon Nanotubes-Graphene Composites by Co-Assembly in Evaporating Droplets for Enhanced Electrochemical Energy Storage, *J. Alloys Compd.*, **751**: 43−48 (2018).

[15] Sakurai H., Daiko T., Hirao T., A Synthesis of Sumanene, a Fullerene Fragment, *Science,* **301**: 1878−1878 (2003).

[16] Barth W. E.; Lawton R. G., A Practical, Large Scale Synthesis of the Corannulene System, *J. Am. Chem. Soc.*, **88**: 380–381 (1966).

[17] Lawton R.G., Barth, W.E., Synthesis of Corannulene, *J. Am. Chem. Soc.,* **93**: 1730–1745 (1971).

[18] (a) Vessally E., Gharibzadeh F., Edjlali L., Eshaghi M., Mohammadi R., A DFT Study on Sumanene, Corannulene and Nanosheet as the Anodes in Li−Ion Batteries, *Iran. J. Chem. Chem. Eng. (IJCCE),* **39(6)**: 51-62 (2020).

(b) Moladoust R., Sensing Performance of Boron Nitride Nanosheets to a Toxic Gas Cyanogen Chloride: Computational Exploring, *Chem. Rev. Lett.*, **2**: 151-156 (2019);

(c) Majedi S., Ghafur Rauf H., Boustanbakhsh M., DFT Study on Sensing Possibility of the Pristine and Al- and Ga-Embedded $B_{12}N_{12}$ Nanostructures Toward Hydrazine and Hydrogen Peroxide and Their Analogues**,** *Chem. Rev. Lett.,* **2**: 176-186 (2019);

(d) Majedi S, Behmagham F., Vakili M., Theoretical View on Interaction Between Boron Nitride Nanostructures and Some Drugs, *J. Chem. Lett.,* **1:** 19-24 (2020).

[19] Chai J.−D., Head−Gordon M., Long-Range Corrected Hybrid Density Functionals with Damped Atom–Atom Dispersion Corrections, *Phys. Chem. Chem. Phys.,* **10**: 6615 (2008).

[20] Frisch M.J., *et.al.,* Gaussian09 Program, Gaussian Inc.,Wal Nangford, CT, (2009).

[21] S.F. Boys, F. Bernardi, The Calculation of Small Molecular Interactions by the Differences of Separate Total Energies, Some Procedures with Reduced Errors, *Mol. Phys.,.*, **19**: 553–561 (1970).

[22] N. O'Boyle, A. Tenderholt, K. Langner, A Library for Package- Independent Computational Chemistry Algorithms, *J. Comput. Chem.*, **29**: 839–845 (2018).

[23] Zuo C., Chen Q., Tian L., Waller L., Asundi A., Transport of Intensity Phase Retrieval and Computational Imaging for Partially Coherent Fields: The Phase Space Perspective, *Optics and Lasers in Engineering*., **71**: 20-32 (2015).

[24] Li X., Feng Y., Liu B., Yi D., Yang X., Zhang W.,... Bai P., Influence of NbC particles on microstructure and Mechanical Properties of AlCoCrFeNi High-Entropy Alloy Coatings Prepared by Laser Cladding, *Journal of Alloys and Compounds.,* **788**: 485-494 (2019).

[25] Wang M., Yang L., Hu B., Liu J., He L., Jia Q., ... Zhang Z., Bimetallic NiFe Oxide Structures Derived from hollow NiFe Prussian Blue Nanobox for Label-Free Electrochemical Biosensing Adenosine Triphosphate, *Biosensors & Bioelectronics.,* **113**: 16-24 (2018).

[26] Liu Y., Xu T., Liu Y., Gao Y., Di C., Wear and heat Shock Resistance of Ni-WC Coating on Mould Copper Plate Fabricated by Laser, *Journal of Materials Research and Technology*, **9(4)**: 8283-8288 (2020).

[27] Wang P., Li Z., Xie Q., Duan W., Zhang X., ... Han H., A Passive Anti-Icing Strategy Based on a Superhydrophobic Mesh with Extremely Low Ice Adhesion Strength, *Journal of Bionic Engineering.*, **18**: 55 -64 (2021).

[28] Chen X., Wang D., Wang T., Yang Z., Zou X., Wang P., ... Wei Z., Enhanced Photoresponsivity of a GaAs Nanowire Metal-Semiconductor-Metal Photodetector by Adjusting the Fermi Level, *ACS Applied Materials & Interfaces*., **11(36)**: 33188-33193 (2019).

[29] Li H., Tang J., Kang Y., Zhao H., Fang D., Fang X., ... Wei Z., Optical properties of Quasi-Type-II Structure in GaAs/GaAsSb/GaAs Coaxial Single Quantum-Well Nanowires, *Applied Physics Letters.,* **113(23)**: 233104 (2018).

[30] Lu H., Zhu Y., Yuan Y., He L., Zheng B., Zheng X., ... Du H., LiFSI as a Functional Additive of the Fluorinated Electrolyte for Rechargeable Li-S **B**atteries, *Journal of Materials Science*, *Materials in Electronics.*, **32(5)**: 5898-906 (2021).

[31] Zhang H., Guan W., Zhang L., Guan X., & Wang S., Degradation of an Organic Dye by Bisulfite Catalytically Activated with Iron Manganese Oxides: The Role of Superoxide Radicals, *ACS Omega.*, **5(29)**: 18007-18012 (2020).

[32] Zhang H., Sun M., Song L., Guo J., & Zhang L., Fate of NaClO and Membrane Foulants During Insitu Cleaning of Membrane Bioreactors: Combined Effect on Thermodynamic Properties of Sludge, *Biochemical Engineering Journal*., **147**: 146-152 (2019).

[33] Sun M., Yan L., Zhang L., Song L., Guo J., ... Zhang H., New Insights into the Rapid Formation of Initial Membrane Fouling after In-Situ Cleaning in a Membrane Bioreactor, *Process Biochemistry* (1991)., **78**: 108-113 (2019).

[34] Liu Z., Wang C., Zhu Z., Lou Q., Shen C., Chen Y., ... Shan C., Wafer-Scale Growth of Two-Dimensional Graphitic Carbon Nitride Films, *Matter*., **4(5)**: 1625-1638 (2021).

[35] Dai Z., Xie J., Chen Z., Zhou S., Liu J., Liu W., ... Ren X., Improved Energy Storage Density and Efficiency of $(1-x)Ba_{0.85}Ca_{0.15}Zr_{0.1}Ti_{0.9}O_3$-$xBiMg_{2.3}Nb_{1.3}O_3$ Lead-Free Ceramics, *Chemical Engineering Journal (Lausanne, Switzerland : 1996).*, **410**: 128341 (2021).

[36] Dai Z., Guo S., Gong Y., & Wang Z., Semiconductor Flexoelectricity in Graphite-Doped $SrTiO_3$ Ceramics, *Ceramics International.*, **47(5)**: 6535-6539 (2021).

[37] Zhang Y., Liu G., Zhang C., Chi Q., Zhang T., Feng Y., ... Cao D., Low-Cost $MgFexMn_2$-xO_4 Cathode Materials for High-Performance Aqueous Rechargeable Magnesium-Ion Hatteries, *Chemical Engineering Journal (Lausanne, Switzerland : 1996).*, **392**: 123652 (2020).

[38] Duan Y., Liu Y., Chen Z., Liu D., Yu E., Zhang X., ... Du H., Amorphous Molybdenum Sulfide Nanocatalysts Simultaneously Realizing Efficient Upgrading of Residue and Synergistic Synthesis of 2D MoS_2 Nanosheets/Carbon Hierarchical Structures, *Green Chemistry : An international Journal and Green Chemistry Resource : GC.*, **22(1)**: 44-53 (2020).

[39] Kang Y., Zhang Y., Shi Q., Shi H., Xue D., ... Shi F., Highly Efficient Co_3O_4/CeO_2 Hetero Structure as Anode for Lithium-Ion Batteries, *Journal of Colloid and Interface Science*., **585**: 705-715 (2021).

[40] Tan L., Sun Y., Wei C., Tao Y., Tian Y., An Y., ... Feng J., Design of Robust, Lithiophilic, and Flexible Inorganic- Polymer Protective Layer by Separator Engineering Enables Dendrite- Free Lithium Metal Batteries with $LiNi_{0.8}Mn_{0.1}Co_{0.1}O_2$ Cathode, *Small (Weinheim an der Bergstrasse, Germany).*, **17(13)**: 2007717 (2021).

[41] Liu C., Deng F., Heng Q., Cai X., Zhu R., ... Liserre M., Crossing Thyristor Branches Based Hybrid Modular Multilevel Converters for DC Line Faults, *IEEE Transactions on Industrial Electronics (1982).*, 1 (2020).

[42] Pan Q., Zheng Y., Tong Z., Shi L., Tang Y., Novel Lamellar Tetrapotassium Pyromellitic Organic for Robust High- Capacity Potassium Storage, *Angewandte Chemie (International ed.).*, **60(21)**: 11835-11840 (2021).

[43] Tong X., Ou X., Wu N., Wang H., Li J., ... Tang Y., High Oxidation Potential ≈6.0 V of Concentrated Electrolyte toward High- Performance Dual- Ion Battery, *Advanced Energy Materials.*, 2100151 (2021).

[44] Yin H., Han C., Liu Q., Wu F., Zhang F., ... Tang Y., Recent Advances and Perspectives on the Polymer Electrolytes for Sodium/Potassium- Ion Batteries, *Small (Weinheim an der Bergstrasse, Germany).*, **28**: 2006627 (2021).

[45] Wu N., Zhou X., Kidkhunthod P., Yao W., Song T., ... Tang Y., K- Ion Battery Cathode Design Utilizing Trigonal Prismatic Ligand Field, *Advanced Materials (Weinheim).*, **9**: 2101788 (2021).

[46] Miao Z., Xiaohe S., Xuewu O., Yongbing T., Rechargeable Batteries Based on Anion Intercalation Ggraphite Cathodes, *Energy Storage Materials.*, **16**: 65-84 (2019).

[47] Chen L., Xu J., Zhang M., Rong T., Jiang Z., ... Li P., Systematic Study on Mechanical and Electronic Properties of Ternary VAlN, TiAlN and WAlN Systems by First-Principles Calculations, *Ceramics International.*, **47(6)**: 7511-7520 (2021).

[48] Wang X., Feng Z., Xiao B., Zhao J., Ma H., Tian Y., ... Tan L., Polyoxometalate-Based Metal–Organic Framework-Derived Bimetallic Hybrid Materials for Upgraded Electrochemical Rreduction of Nitrogen, *Green Chemistry : An International Journal and Green Chemistry Resource : GC.*, **22(18)**: 615769 (2020).

[49] Wang R., Yuan Y., Zhang J., Zhong X., Liu J., Xie Y., ... Xu Z., Embedding Fe_2P Nanocrystals in Bayberry-Like N, P-Enriched Carbon Nanospheres as Excellent Oxygen Reduction Electrocatalyst for Zncair Battery, *Journal of Power Sources*., 501: 230006 (2021).

[50] Li H., Xu B., Lu G., Du C., Huang N., Multi-Objective Optimization of PEM Fuel Cell by Coupled Significant Variables Recognition, Surrogate Models and a Multi-Objective Genetic Algorithm, Energy *Conversion and Ianagement*., **236**: 114063 (2021).

[51] Li H., Gao Y., Du C., Hong W., Numerical Study on Swirl Cooling Flow, Heat Transfer and Stress Characteristics Based on Fluid-Structure Coupling Method under Different Swirl Chamber Heights and Reynolds Numbers, *International Journal of Heat and Mass Transfer*., **173**: 121228 (2021).

[52] Simos T. E., Tsitouras C., 6th Order Runge-Kutta Pairs for Scalar Autonomous IVP, Applied and Computational Materials, *Applied and Computational Nathematics,* **19(3):** 412-421(2020).

[53] Jalali Sarvestani M. R., Charehjou P., Fullerene (C20) as a Potential Adsorbent and Sensorfor the Removal And Detection of Picric Acid Contaminant: DFT Studies, *Cent. Asian J. Environ. Sci. Technol. Innov.,* **2**: 12-19 (2021).

[54] Rasouli A., Bafkar A., Chaghakaboodi Z., Kinetic and Equilibrium Studies of Adsorptive Removal of Sodium-Ion onto Wheat Straw and Rice Husk Wastes, *Cent. Asian J. Environ. Sci. Technol. Innov.,* **1**: 310-329 (2020).

[55] Ali A., Iqbal M. M., Waheed A., Co-treatment of chlorophenol and methanolic wastes, *Cent. Asian J. Environ. Sci. Technol. Innov.,* **1**: 277-280 (2020).

[56] Bafkar A., Kinetic and Equilibrium Studies of Adsorptive Removal of Sodium-Ion onto Wheat Straw and Rice Husk Wastes, *Cent. Asian J. Environ. Sci. Technol. Innov*., **1**: 310-329 (2020).

[57] Awan B., Sabeen M., Shaheen S., Mahmood Q., Ebadi, A., Toughani, M. Phytoextraction of Zinc Contaminated Water by *Tagetes minuta* L., *Cent. Asian J. Environ. Sci. Technol. Innov.,* **1**: 150-158 (2020).

[58] Qayyum, S., Khan I., Meng K., Zhao Y., Peng C., A Review on Remediation Technologies for Heavy Metals Contaminated Soil, *Cent. Asian J. Environ. Sci. Technol. Innov.,* **1**: 21-29 (2020).

[59] Hidehiro S., Taro D., Hiroyuki S., Toru A., Toshikazu H., Structural Elucidation of Sumanene and Generation of Its Benzylic Anions, *J. Am. Chem. Soc.,* **127**: 11580 −11581, (2005).

[60] Scott L.T., Hashemi M.M., Bratcher M.S., Corannulene Bowl-to-Bowl Inversion is Rapid at Room Temperature, *J. Am. Chem. Soc.*, **114(5)**: 1920–1921 (1992).

[61] Denis P.A., Iribarne F., Theoretical Investigation on the Interaction Between Beryllium, Magnesium and Calcium with Benzene, Coronene, Cirumcoronene and Graphene, *Chem. Phys. Lett.*, **573**: 15−18 (2013).

[62] Gao Z., Chin C. S., Chiew J. H. K., Zhang J.J.C., A DFT Study on Nanocones, Nanotubes (4, 0), Nanosheets and Fullerene C 60 as Anodes in Mg-Ion Batteries, *Energy*., **10**: 1503 (2017).